Evaluation of the three-dimensional configuration of a subsurface artificial fracture by the triaxial shear shadow method

doi: 10.1190/1.1443026

GEOPHYSICS, VOL. 56, NO. 12 (DECEMBER 1991); P. 2118–2128, 14 FIGS., 2 TABLES.

Evaluation of the three-dimensional configuration of a subsurface artificial fracture by the triaxial shear shadow method

Hiroaki Niitsuma* and Hiroyuki Saito*

ABSTRACT

We have determined the three-dimensional configuration of a single fracture in the hot dry rock model field at Higashi-Hachimantai, Japan, by the triaxial shear shadow method. The crack was created by hydraulic fracturing in intact welded tuff at a depth of 370 m. We have carried out crosshole seismic measurements by using a downhole air gun and a triaxial seismic detector. Extinction at a special polarization direction and the dependency of transmissivity in shear wave component on incident angle were determined by a triaxial hodogram analysis of detected signals. We have evaluated the orientation and distribution of the fracture using the shear wave extinction, and the three-dimensional configuration of the fracture by a continuation of the evaluated orientations. The results are in good agreement with the data obtained by independent experiments in the field.

INTRODUCTION

Precise evaluation of the configuration and characteristics of subsurface cracks is essential for the structural integrity assessment of an underground cavern and for the creation and use of artificial fractures in modern geothermal developments. The crosshole seismic measurement is one of the most promising techniques for mapping the distribution of underground fractured zones, and many efforts are underway in both theoretical and field studies of the technique. Shear shadowing is one of the techniques and was employed by Aamodt et. al. (1977) and Albright et. al. (1978; 1980) to study the structure of the hot dry rock geothermal reservoir at Fenton Hill, New Mexico. They observed shear-wave attenuation which depends on the absence or presence of fractures along the signal travel paths, and showed the feasibility of the method.

A triaxial detection of the particle motion of the shear-wave component and its hodogram analysis in the crosshole measurement, ie., the triaxial shear shadow method, potentially enables the detection of not only the presence of subsurface fractures but also their orientation, since polarization and amplitude of the transmitted shear wave is highly dependent upon incidence angle. We have studied the method and performed a successful field measurement to determine the three-dimensional configuration of a subsurface artificial fracture in a hot dry rock model field at Higashi-Hachimantai, Japan, where a single fracture was created by the hydraulic fracturing of intact rock. In this paper, we will discuss the methods to determine crack orientation by triaxial hodogram analyses, and we will demonstrate their feasibility showing some experimental results in the field.

DESCRIPTION OF THE METHOD

Description of model

We consider the incidence of an elastic plane wave on a water-filled single crack in isotropic media shown in Figure 1. We assume the crack to be a parallel solid/fluid/solid interface. The wavelength is assumed to be much greater than the thickness of the fluid layer and much less than the crack size. In the figure, **n** represents the unit vector normal to the crack plane and α is the incidence angle. **P** is a direction of wave propagation, $\mathbf{SH}_k$ is a direction of shear-wave particle motion parallel to the crack surface, and $\mathbf{SV}_k$ is the direction of particle motion perpendicular to the SH_k component. Fehler (1982) made a study of the transmission of plane waves through the layered viscoelastic material and showed that the viscosity of the fluid can be assumed to be zero under a condition of the normal crosshole seismic measurement of the water-filled crack.

Manuscript received by the Editor January 2, 1990; revised manuscript received May 3, 1991.
*Department of Resources Engineering, GEEE, Faculty of Engineering, Tohoku University, Sendai 980, Japan.

Determination of crack orientation through measurement of shear wave extinction directions

The SH_k component of the incident shear wave is not transmitted at the solid/fluid/solid interface, providing that the viscosity of the fluid is negligible. Therefore, the transmitted shear wave is polarized in the SV_k direction. The direction is detectable by a crosshole measurement using an impulsive wave source, where the triaxial particle motion at the onset of the transmitted shear wave is detected and analyzed in a plane perpendicular to the P direction. The direction should be determined in a time window before the arrival of the refracted wave around the edge of the crack. In this regard, the difference of path length between transmitted and refracted waves should be greater than a quarter of the wavelength.

SH_k direction is determined as a direction perpendicular to the SV_k direction. Knowing two different SH_k directions $\mathbf{SH}_{k1}$, $\mathbf{SH}_{k2}$ by a measurement for two different raypaths, the crack direction **n** is obtained as a vector product of $\mathbf{SH}_{k1}$ and $\mathbf{SH}_{k2}$ (Figure 2a). In a particular case where $\mathbf{SH}_{k1}$ and $\mathbf{SH}_{k2}$ have the same direction, we cannot determine **n** uniquely. A practical procedure is to determine **n** from several $\mathbf{SH}_k$ vectors by employing the principal component analysis (see Appendix).

If there is no crack between the source and detector, the polarization direction of the observed shear wave coincides with that of the wave source. Then, the nominal SH_k direction is equal to the SH direction and is independent of raypath, when a cylindrical wave source is used.

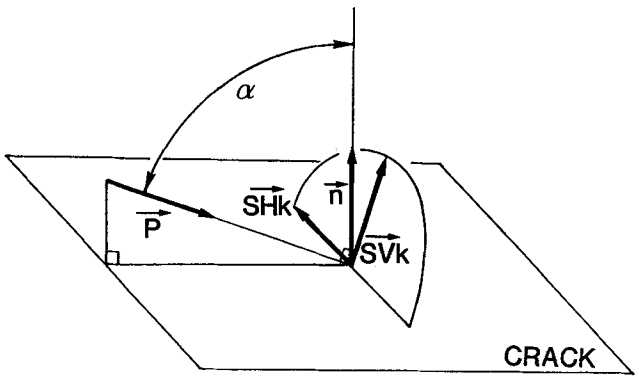

FIG. 1. Incidence of elastic plane wave to a water-filled single crack.

Determination of crack orientation using the shear wave extinction direction and transmissivities

The above mentioned method is unreliable when the SH_k vectors for the different raypaths have almost the same directions. An alternative way to estimate the crack orientation in that case is to analyze the SV_k component. The transmissivity of the SV_k component at the solid/fluid/solid interface is a function of the incident angle α as illustrated in Figure 3 (Fehler, 1982), where T_P and T_{SVk} are the transmissivity of the particle velocity of the P and SV_k components, respectively.

We assume that the directions of the SH_k vectors for adjacent raypaths are the same and can be represented as an average of the observed SH_k directions. The relative incident angles between raypaths $\Delta\alpha_n$ can be calculated, knowing the positions of the wave source and the detector, the averaged SH_k direction, and one of the incident angles α_0. If we can determine the relative transmissivities T_{SVk}/T_P for several raypaths, we can plot them as a function of $\alpha_0 + \Delta\alpha_n$ in the experiment. Then, α_0 can be evaluated by fitting a value of α_0 for the plotted data to fit the theoretical curve. The crack direction **n** is estimated from the α and the SH_k direction (Figure 2b).

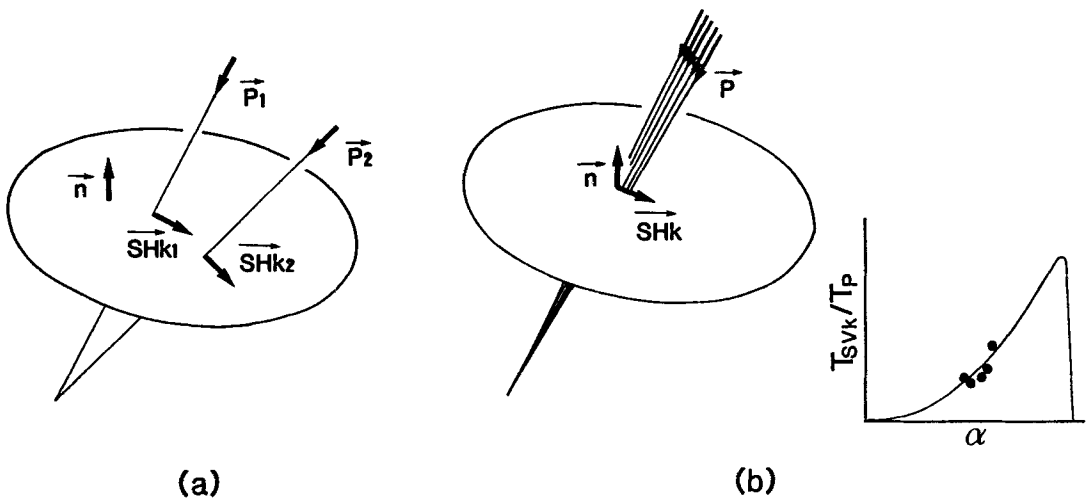

FIG. 2. Principle of the determination of crack orientation by triaxial shear wave analysis. (a) Determination by detecting shear wave extinction directions; (b) determination by detecting a shear wave extinction direction and transmissivities.

Problems with practical measurements

There are several problems with practical shear shadow measurements. We have discussed the question of a single fluid layer in isotropic media as a crack model and have assumed that the wavelength is much greater than the thickness of the fluid layer and much less than the crack size. The validity of the model becomes a matter of concern in the practical measurements.

The face of the fracture is, in general, not flat and smooth but irregular with many contacts. Since the transmissivity of the SH_k wave is dependent on the state of the face, the method is not always applicable for every type of fracture. It is also difficult to evaluate small fractures and the edge of fractures by the method because of the effect of diffraction. We also assume an isotropic media. So, it is necessary to make some corrections when the ray bending cannot be neglected. The method would also be affected by multiple fractures. Basically, the orientation of the closest crack to the detector is evaluated in the first method, and the second method is severely affected by the presence of multiple fractures.

The second problem is associated with the radiation pattern of the compressional and shear wave components in a wave source. A cylindrical wave source such as an air gun generates P- and SV-waves that have very strong directivities. It is advisable that the positions of source and detector should be chosen such that signals would contain significant shear wave component. Moreover, we must take into account the directivity of energy ratio of compressional and shear wave components in the evaluation of the relative transmissivity T_{SVk}/T_p for the second method. The difference in propagation loss between compressional and shear wave also affects the evaluation of T_{SVk}/T_p.

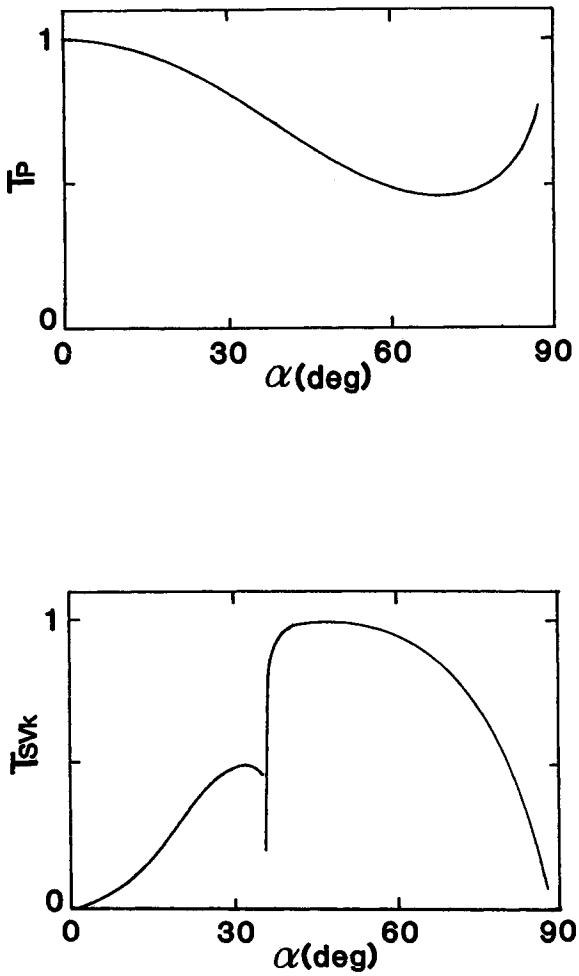

FIG. 3. Transmissivities of P and SV_k waves and relative transmissivity at the solid/fluid/solid interace as a function of incident angle (Fehler 1982).

FIELD AND EXPERIMENTAL SETUP

A triaxial shear-shadowing experiment was carried out in the Higashi-Hachimantai hot dry rock model field in Iwate Prefecture, Japan, which was developed as a part of the Γ-Project of Tohoku University (Niitsuma, 1989a). Figure 4 is an illustration of the field. Six boreholes were drilled into an intact welded tuff. The tuff consists of rhyolitic-dacitic welded tuffs. The welded tuffs, firmed under high temperature, possess properties similar to igneous rocks. A microscopic view of the welded tuff showed a vitreous texture and no preexisting weakness was observed. The temperature of the formation is about 60° C at 370 m depth. It was confirmed by continuous coring that there are no significant natural fractures or joints occurring in the welded tuff in the 280–380 m depth interval.

An artificial single fracture was created at 369.0 m in the F-1 well by hydraulic fracturing. A total volume of 7400 l of gel with 20/40 mesh proppant was injected during the fracturing. The injected volume corresponds to a propped crack of about 50 m diameter. The EE-4 well was drilled after the fracturing by continuous coring and the F-1 and EE-4 wells were connected through the artificial fracture, forming a circulation system. A core of a part of the fracture obtained at 358.2 m in the EE-4 well, revealed that the normal direction of the fracture plane is almost perpendicular to the minimum principal stress evaluated by a three-dimesional tectonic stress measurement in the field (Hayashi et al., 1985). A circulation test of the system indicates that the fracture has a finite aperture of 0.1–0.2 mm near the F-1 and EE-4 well without pressurization (Hayashi, 1989).

The velocity structure of the field was also determined by a calibration test for downhole acoustic emission measurements (Sato et al., 1986). The velocities of the compressional and shear waves are almost constant in the 280–380 m depth interval, and are about 2710 m/s and 1730 m/s, respectively. No shear-wave splitting effect was recognized in the welded tuff by the measurement.

Triaxial shear-shadowing experiments were performed to determine the three-dimensional configuration of the artificial fracture. We modified an air gun (Bolt, DHS-5500) for downhole use and used it as a wave source. The energy of the wave was distributed mainly in the frequency range of 100–500 Hz. A downhole triaxial acoustic emission sonde (Niitsuma, 1989b) was employed as a detector. The sonde

consists of triaxial piezoelectric accelerometers, preamplifiers, an electronic compass, and two mechanical coupling devices. The devices have two mechanical arms driven by gear motors and are set at the upper and lower parts of the sonde. By using the sonde, triaxial particle motion can be detected at a frequency range of 7–400 Hz.

Preliminary measurements were carried out before and after the hydraulic fracturing. The air gun was deployed at 210–370 m depth interval of F-1 well and the detector at a depth of 295 m in E-3 well. The distance between the source and the detector varied from 29 to 100 m.

A detailed measurement was carried out after the drilling of EE-4 well, using F-1, E-3, and EE-4 wells. The artificial fracture was not pressurized in the experiment. The sonde was set in the open hole section of E-3 well (300–380 m), while the wave source was set in the 285–362 m depth interval of EE-4 well and in the 321–358 m of F-1 well. The arrangement of the source and the detector in this experiment is shown in Figure 5. The distance between the source and the detector was 26–70 m. The tectonic stress measurements lead us to believe that the artificial fracture would occur between the three boreholes.

SIGNAL PROCESSING

Detected signals were digitized and processed with a computer, and a flow chart is shown in Figure 6. Stacking of three to ten signals for each raypath was made before analyses. A transformation of coordinates from X, Y, Z to P, SH, SV system was carried out for the stacked triaxial signals. Then, hodogram analyses were made on the SH-SV plane in order to detect the onset of the shear wave and to measure the SH_k direction. An example of the triaxial signal and its hodogram in SH-SV plane are shown in Figure 7. It was known empirically that the onset of the shear wave would be recognizable as a linear motion of the hodogram in the SH-SV plane (② → ③ → ④); before that, circular motions are observed in the coda of the compressional wave. The SV_k and SH_k directions were determined at the onset of the shear wave as shown in the figure. After a coordinates

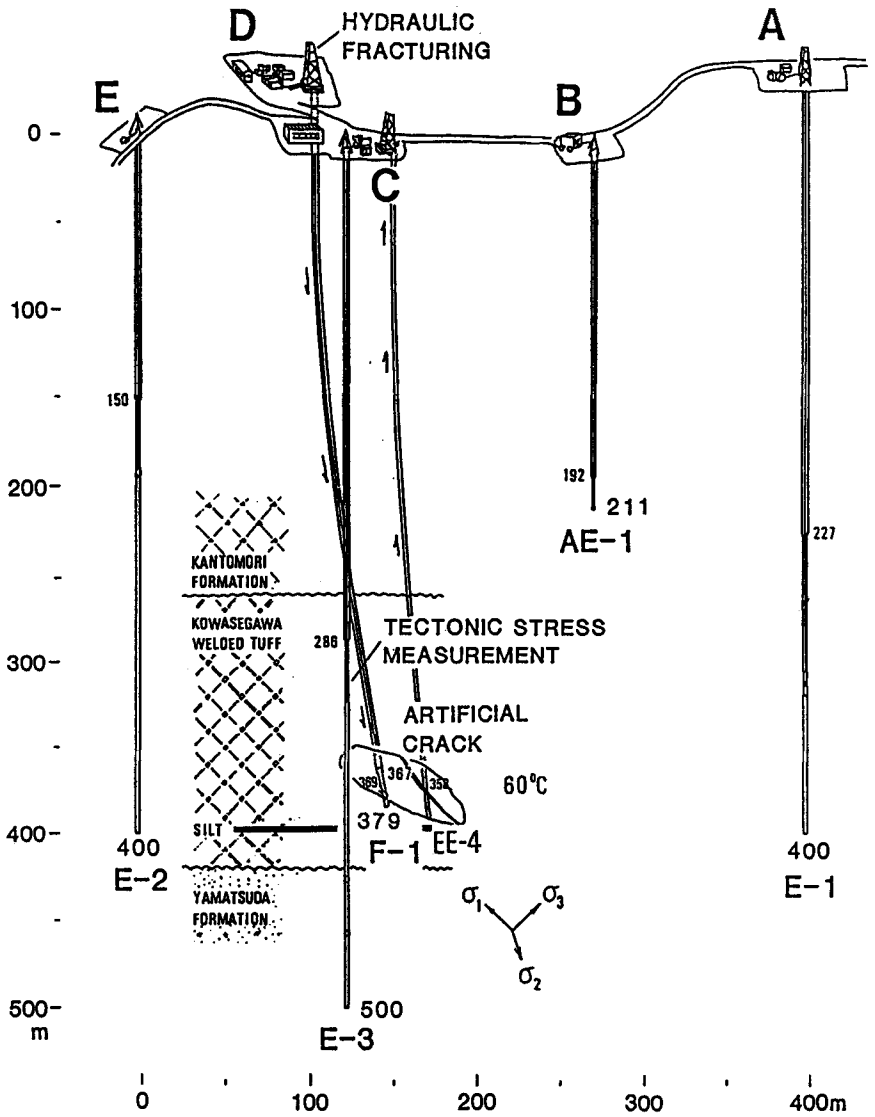

FIG. 4. Higashi-Hachimantai hot dry rock model field.

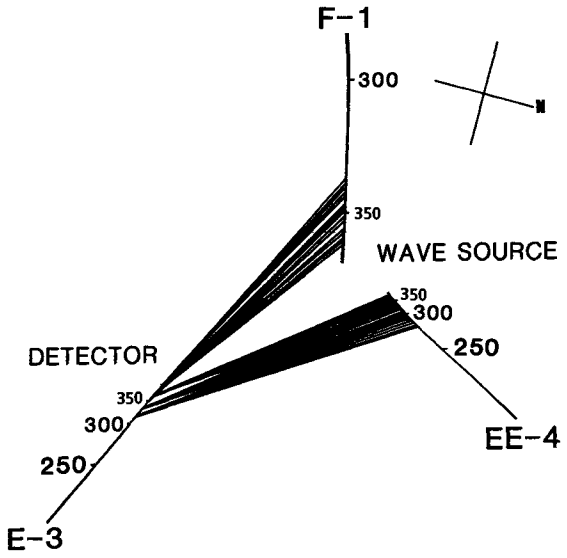

FIG. 5. Arrangement of the wave source and the detector.

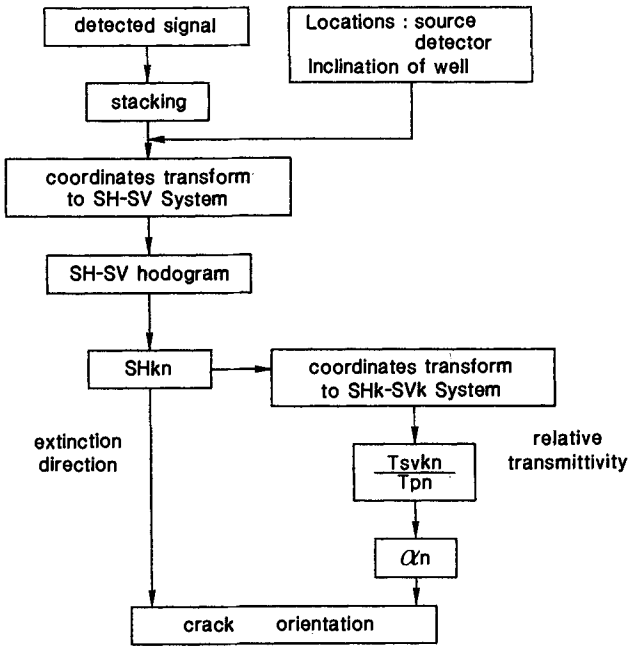

FIG. 6. Processing flow of the triaxial shear shadow analysis.

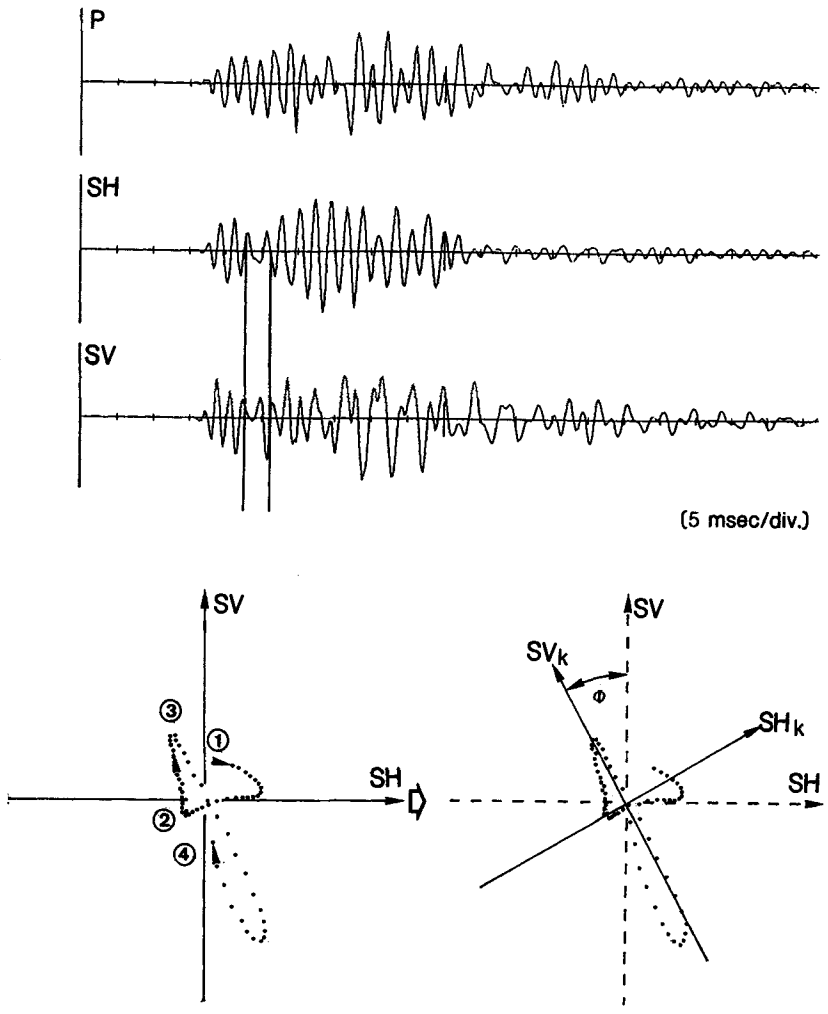

FIG. 7. Detected shear-shadowed signal and its *SH-SV* hodogram at the onset of shear wave. ② shows the onset of shear wave.

transformation from P, SH, SV to P, SH_k, SV_k system, the relative transmissivity T_{SVk}/T_P at the onset of shear wave was determined. The distribution of crack directions was estimated by the two methods described before.

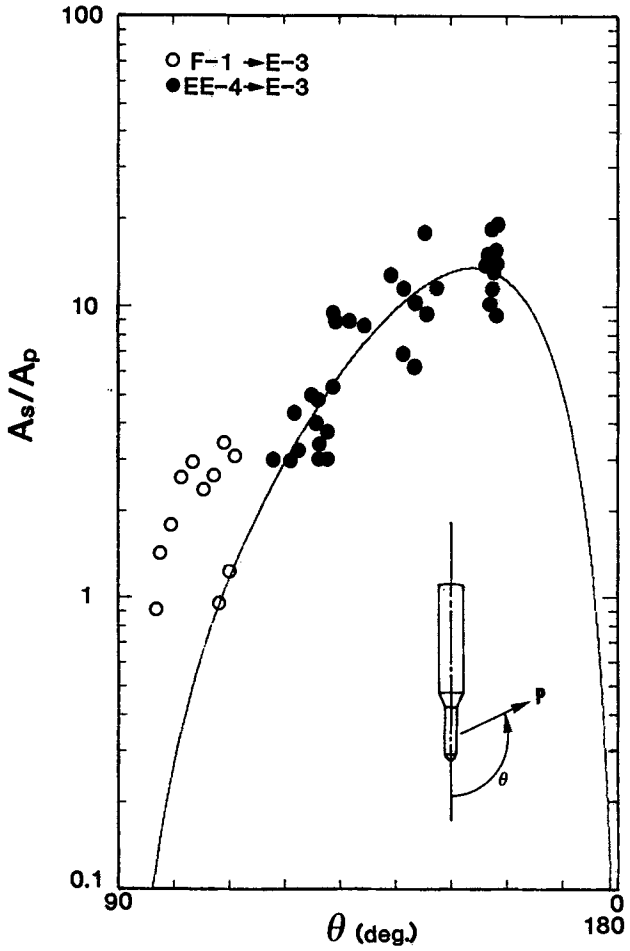

FIG. 8. Radiation pattern of the downhole air gun.

RESULTS

Preceding the shear-shadowing experiments, we measured the radiation pattern of the air gun. As mentioned above, the radiation pattern is an important factor not only for selection of the source and detector positions but also for evaluation of the relative transmissivity T_{SVk}/T_P. The radiation pattern should also be taken into account in the detection of shear-shadowed sections where evaluation of relative amplitude A_{SHk}/A_P has an advantage over evaluation of absolute shear wave amplitude A_{SHk}, because the absolute amplitude is highly dependent on the condition of the borehole and on a pressure difference between the air gun chamber and the borehole. The result is shown in Figure 8. The abscissa is the angle θ between the propagation direction and the axis of the air gun, and the ordinate is the relative amplitude A_S/A_P of the detected signals. The closed circles show data on ray-paths from EE-4 to E-3, and open circles from F-1 to E-3. All paths were chosen so as not to intersect the artificial fracture. The solid lines in the figure are the theoretical curve for cylindrical wave source by Fehler and Pearson (1981), represented as follows:

$$\frac{A_S}{A_P} \equiv R(\theta) = K \frac{\sin\theta \cos\theta}{2 - \cos^2\theta}, \tag{1}$$

where K is a constant. Although scattering and deviation is observed, the data correspond well to the theoretical curve when we set $K = 5.27$. The deviation of the data on F-1 → E-3 from the data on EE-4 → E-3 is considered to be due to the difference in borehole diameter, casing, and cementing in the F-1 well. The relative transmissivity T_{SVk}/T_P was calculated as follows using the theoretical curve $R(\theta)$:

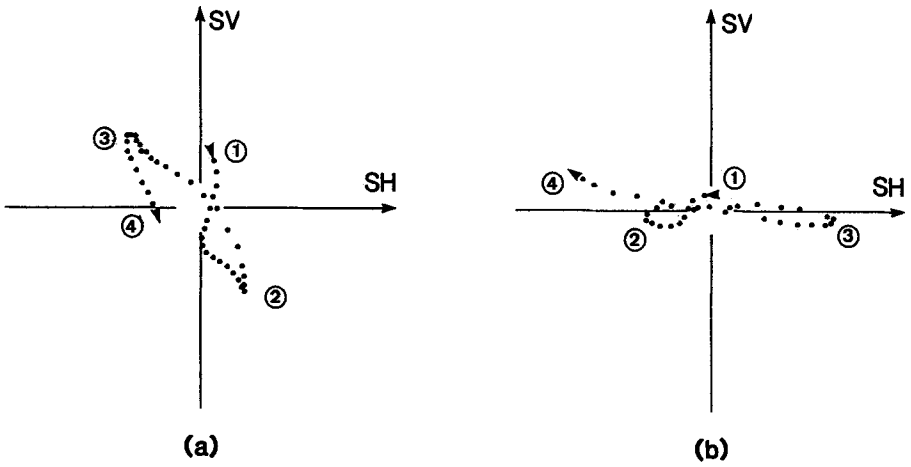

FIG. 9. Hodograms at the onset of the S wave in SH-SV plane before and after the fracturing.

$$\frac{T_{SVk}}{T_P} = R(\theta)\,\frac{A_{SVk}}{A_P}, \qquad (2)$$

where A_p is the amplitude at the onset of the P wave and A_{SVk} is that of the SV_k wave.

A result of the preliminary experiment is shown in Figure 9, where the hodograms at the onset of the S wave in the SH-SV plane both before and after the fracturing for an identical raypath are shown. Considerable changes of S-wave polarization were observed in the preliminary experiments, suggesting a creation of the artificial fracture, although the data was insufficient to evaluate the configuration of the fracture because of trouble with the hardware and improper arrangements of the wave source and detector.

Results of the detailed measurement after the drilling of EE-4 well are shown in Figures 10–14. Figure 10 shows a change of waveform with depth of the wave source in the EE-4 well. The detector was fixed at a depth of 377.8 m in the E-3 well in the experiment. The signals were coordinate transformed to P, SH_k, SV_k system according to the flow chart shown in Figure 6, where the SH_k directions were detected for every stacked signal. The broken lines show arrival of the compressional wave and dotted lines that of the shear wave. Anomalous extinctions at the arrival of the shear wave are observed in the SH_k component below the depth of 321 m, while the amplitude of SV_k component changes depending on the depth.

We determined the shear-shadowed sections, considering the change of SH_k and SV_k component, as well as the directivity of wave source. Figure 11 shows a result, where dotted areas indicate sections at which shear-shadowing was observed.

The triaxial analyses were performed for the shear-shadowed sections. Figure 12 shows examples of a stereographic projection of detected SH_k directions for the sections. The solid lines in the figure show most probable planes that would contain all the vectors evaluated by the principal component analysis. As shown in the figure, we can reasonably determine the planes. Table 1 shows estimated crack orientations by the method of detecting SH_k directions. The strike and dip were evaluated by the principal component analysis of SH_k vectors for five different raypaths. As shown in the table, the evaluated orientations have the same approximate direction as that of the core sample of the artificial fracture (N61E, NW46) and that estimated by the tectonic stress measurement (N85E, NW 49.7).

The dependency of shear-wave transmissivity on incident angle was also observed for the shear-shadowed signals. Figure 13 shows some results of the fitting of the observed relative transmissivity to the theoretical curve. The incident angles are reasonably determined by the fitting for some data, while scattering is too extensive to determine an incident angle for others. Table 2 shows crack orientations estimated by the second method through measurement of SH_k directions and relative transmissivities. Although estimated orientations have the same tendency as those estimated by the first method, considerable difference for several raypaths is observed. Crack orientation could not be determined by the second method for the experiment where the air gun was set in the F-1 well because of significant scattering of the relative transmissivities. That is considered to be due to the effects of casing and cementing, as well as the effect of multiple cracks.

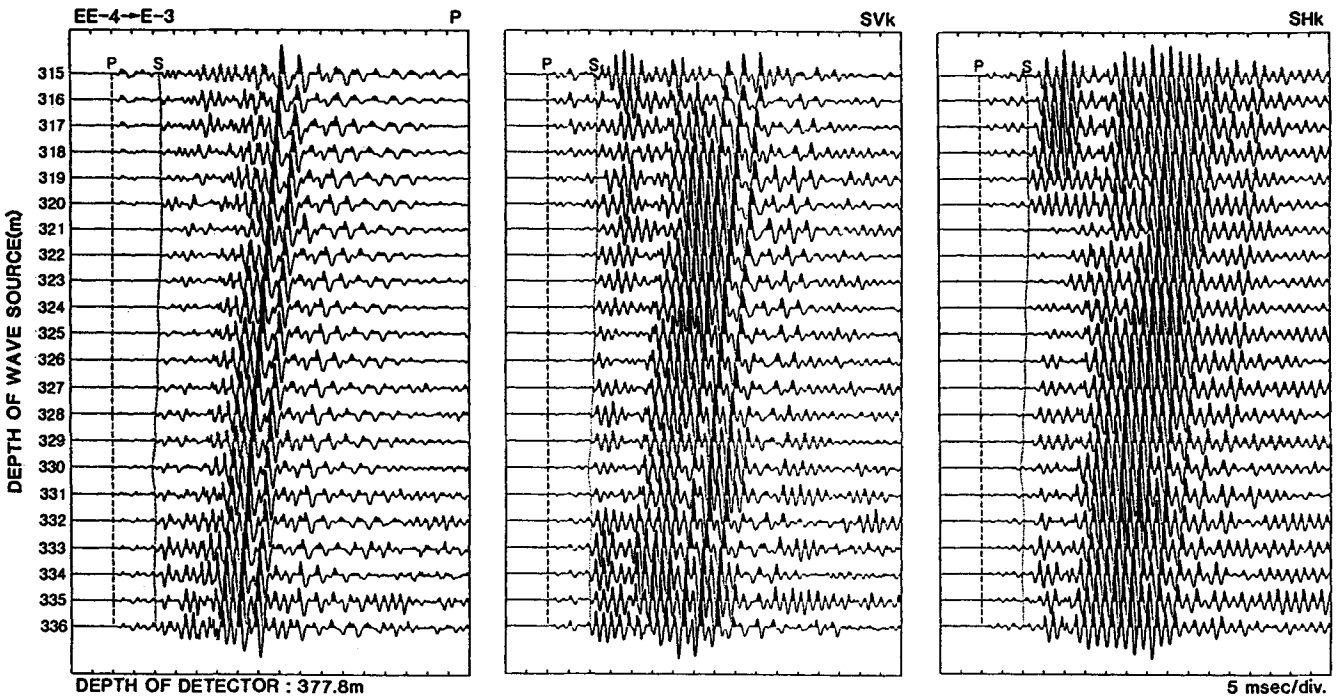

FIG. 10. Change of P, SV_k, and SH_k waveforms with depth of wave source in EE-4 well. Detector was fixed at a depth of 377.8 m in E-3 well.

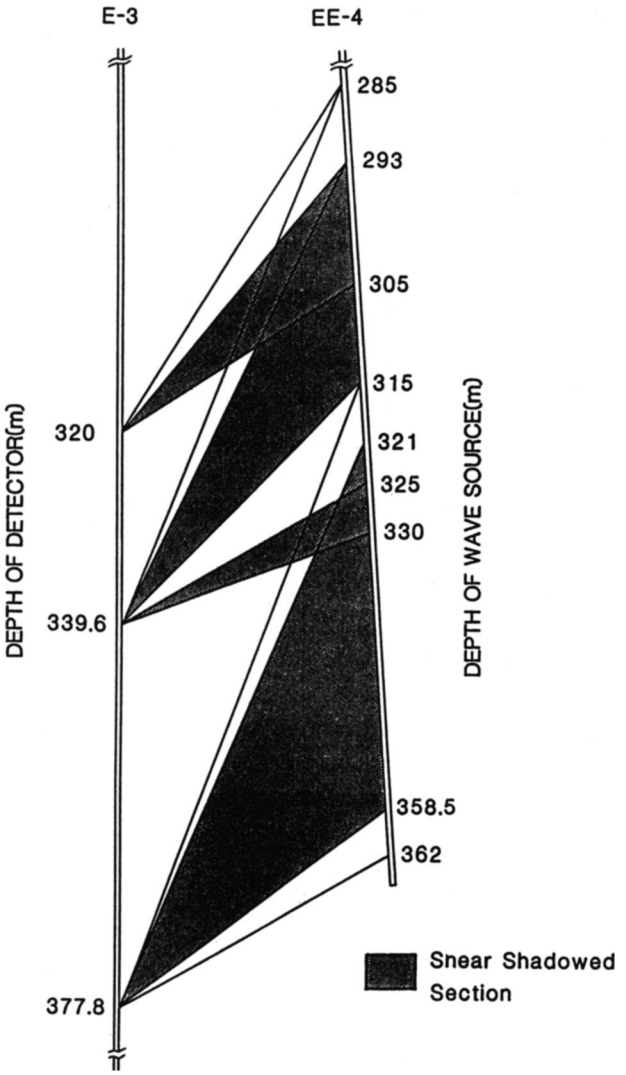

FIG. 11. Detected shear-shadowed sections.

Table 1. Crack orientations estimated by a principal component analysis of detected SHk directions.

Wave Source (m)		Detector (m)		Strike (deg.)	Dip (deg.)
EE-4	285.0~295.0	ES-3	320.0	*	
	297.0~305.0			N50.6E	NW60.3
	285.0~289.0		339.6	*	
	291.0~304.0			N67.0E	NW24.9
	295.0~313.0			N58.3E	NW35.4
	313.0~321.0			*	
	323.0~330.0			**	
	315.0~320.0		377.8	*	
	321.0~325.0			N63.9E	NW23.7
	326.0~330.0			N61.8E	NW28.7
	331.0~335.0			N61.3E	NW30.5
	336.0~340.0			N61.5E	NW34.7
	341.0~345.0			N60.7E	NW39.4
	346.0~350.0			N62.3E	NW40.9
	350.5~352.5			N62.5E	NW44.0
	353.0~355.5			N59.4E	NW51.8
	355.5~358.0			N63.4E	NW52.2
	358.5~362.0			*	
F-1	321.0~328.0	E-3	317.2	*	
	321.0~325.0		330.0	N36.8E	NW75.2
	325.0~329.0			N36.0E	NW83.2
	333.0~336.0			N39.7E	NW81.5
	337.0~341.0			*	
	333.0~337.0		344.6	N40.2E	NW70.4
	337.0~341.0			N42.3E	NW79.5
	346.0~350.0			N42.9E	NW84.6
	350.0~354.0			N45.1E	NW74.5
	346.0		357.2	*	
	347.0~353.0			N43.9E	NW76.7
	354.0			*	
	350.0~352.0		365.0	N49.2E	NW66.5
	352.0~354.0			N49.2E	NW67.7
	354.0~356.0			N42.0E	NW63.1
	356.0~358.0			N47.1E	NW68.7

* :no shear shadow
** :impossible to detect SHk direction the core sample at EE-4 358.2m: N61E NW46 estimation by the 3-D stress measurement: N85E NW49.7

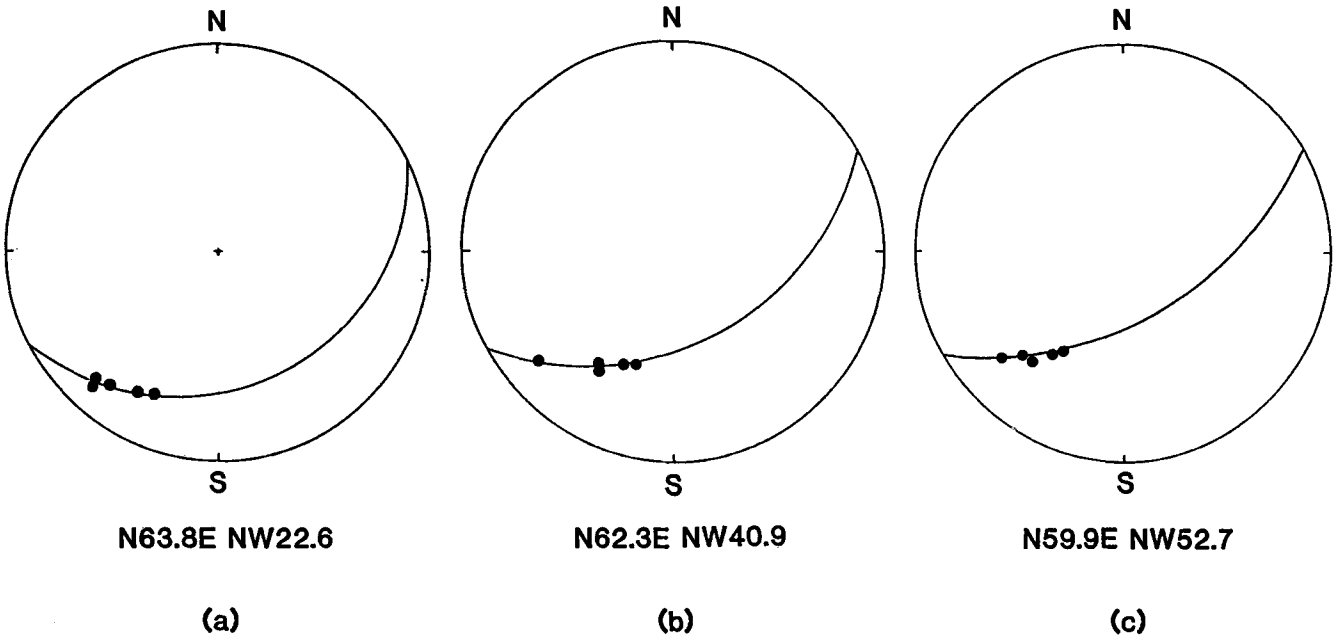

FIG. 12. Examples of stereographic projections of detected SH_k directions for the shear-shadowed sections.

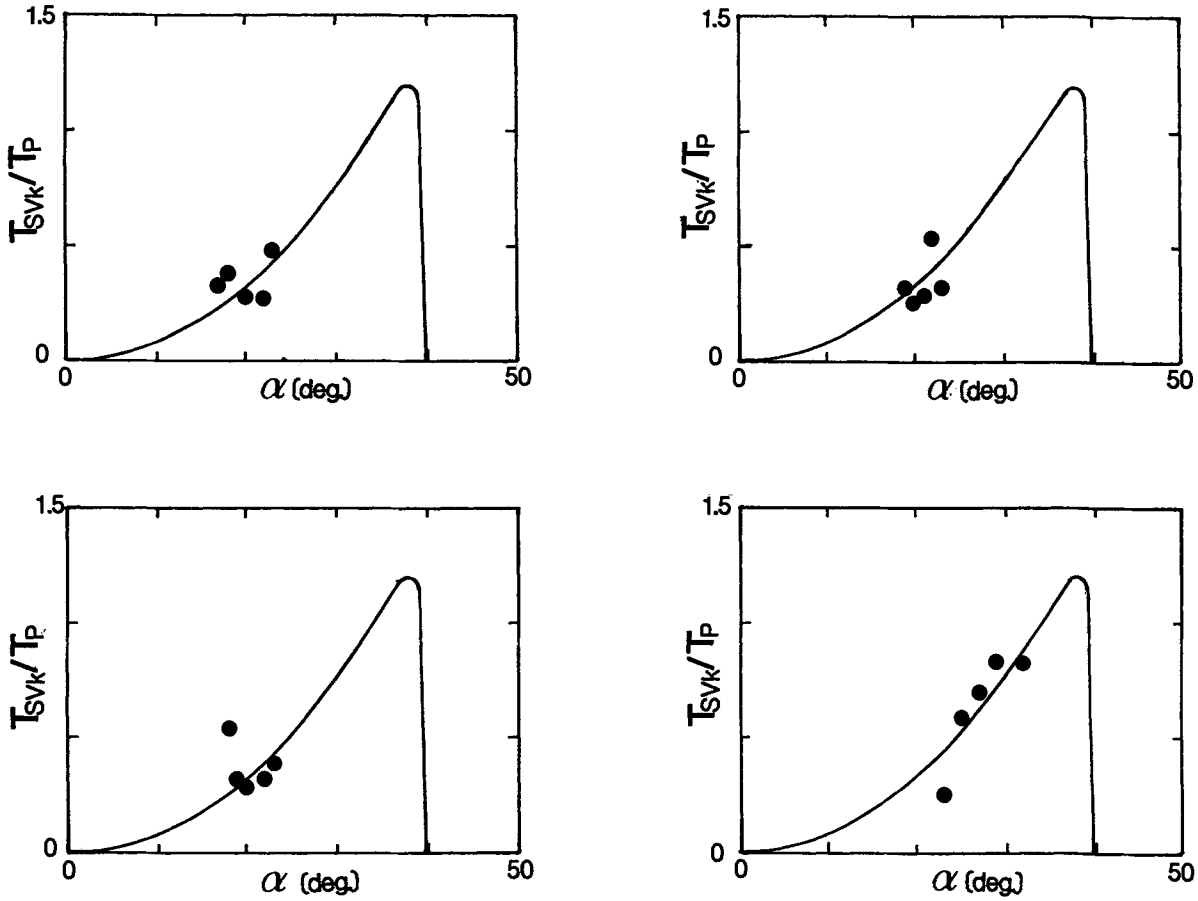

FIG. 13. Examples of the incident angle dependency of detected shear wave transmissivity.

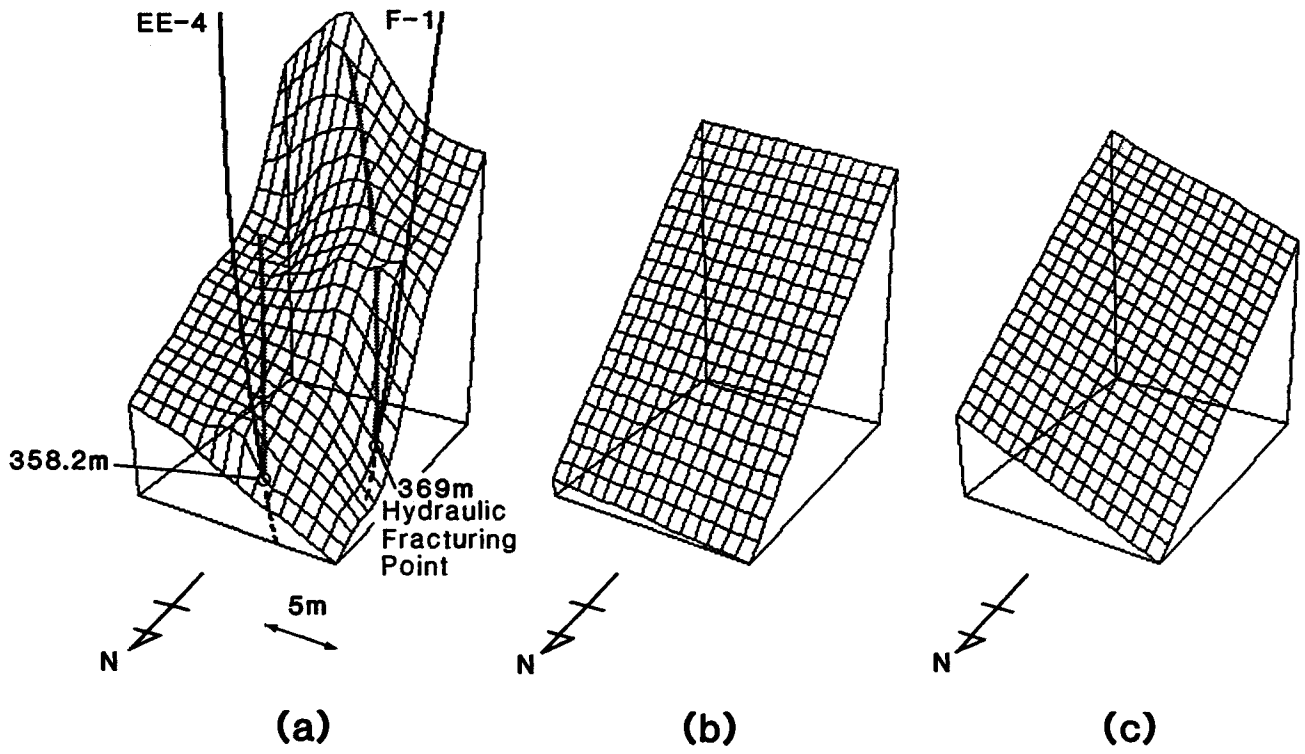

FIG. 14. Estimated three-dimensional configuration of the artificial crack. (a) Configuration by the triaxial shear shadow method, (b) crack orientation estimated by the three-dimensional tectonic stress measurement, (c) orientation of the core sample of the crack at 358.2 m depth in EE-4.

Table 2. Crack orientations estimated from SHk directions and shear wave transmittivities.

Wave Source (m)		Detector (m)		Strike (deg.)	Dip (deg.)
EE-4	285.0~295.0	E-3	320.0	*	
	297.0~305.0			N85.1E	NW52.9
	285.0~289.0		339.6	*	
	291.0~305.0			N50.5E	NW47.0
	299.0~313.0			N49.0E	NW50.8
	313.0~321.0			*	
	323.0~330.0			**	
	315.0~320.0		377.8	*	
	321.0~325.0			N50.7E	NW50.2
	326.0~331.0			N66.8E	NW46.7
	331.0~336.0			N66.7E	NW45.1
	336.0~342.0			N64.2E	NW44.3
	343.0~349.0			N52.6E	NW42.5
	348.0~352.0			N72.6E	NW58.9
	352.5~355.0			N50.0E	NW44.5
	355.5~358.0			N72.4E	NW54.7
	358.5~362.0			*	

* :no shear shadow
** :impossible to detect SHk direction

We can estimate a three-dimensional distribution of the fracture by a continuation of the evaluated orientations, knowing the intersections of the boreholes and the fracture. Figure 14 shows an estimated three-dimensional configuration of the fracture. The orientations were evaluated by the method using several SH_k directions. A crack plane derived from the three-dimensional tectonic stress measurement (Figure 14b) and an orientation of the core sample of the crack (Figure 14c) are also shown. The orientation estimated by the triaxial shear shadow method is almost the same as that of the core sample near the EE-4 well, and the general tendency corresponds well to that estimated by the tectonic stress measurement. The observed shear-shadowed sections are indicated by the hatched lines in Figure 14a, the lengths of which are 30.6 and 18.5 m. The distribution of shear-shadowed areas is reasonable, considering that the size of the fracture is estimated to be about 50 m from the volume of the injected proppant. The size is about eight to ten times that of the wavelength.

CONCLUSIONS

The three-dimensional configuration of the artificial single fracture in intact rock has been successfully determined by the triaxial shear shadow method.

Extinction at a special polarization direction and the dependency of transmissivity on incident angle were observed in the transmitted shear wave. We have evaluated the orientation and distribution of the fracture from the shear wave extinction directions. The result is in good agreement with the core sample data and the expectation through the in-situ tectonic stress measurement. The method using the extinction directions is effective when raypaths can be taken such that the extinction directions differ from each other.

The incident angle dependency can also be used for evaluation of fracture orientation. The result of the second method is also consistent with the core sample data. However, the method is affected by multiple cracks and changes of wave source efficiency and propagation losses. Therefore, the second method should be employed to complement the first method.

Continuation of the evaluated crack orientations can reveal a three-dimensional configuration of a subsurface fracture. The evaluated configuration is in good agreement with the core sample data and the expectation through the in-situ tectonic stress measurement. The estimated size of the fracture also corresponds well with that estimated from the volume of the injected fluid with proppant.

ACKNOWLEDGMENT

The authors wish to express their thanks to Mr. M. Ejiri for his assistance on this research. The work presented here was supported by the Ministry of Education, Science, and Culture under Grant-in-Aid for General Scientific Research 62550295.

REFERENCES

Aamodt, R. L., 1977, Hot dry rock geothermal energy development project, Ann. Rep. FY 1977, Los Alamos Scientific Laboratory Rep., LA-7109-PR, 97-106.

Albright, J. N., Aamodt, R. L., Potter, R. M., and Spence, R. W., 1978, Acoustic method for detecting water-filled fractures using commerical logging tools: Proc. 4th Ann. DOE Symp., Enhanced Oil & Gas Recovery & Improved Drilling Methods, **2**, F-6/1–13.

Albright, J. N., Pearson, C. F., and Fehler, M. C., 1980, Transmission of acoustic signals through hydraulic fractures: Prof. of SPWLA 21st Ann. Logging Symp.

Fehler, M., 1982, Interaction of seismic waves with a viscous liquid layer: Bull. Seis. Soc. Am., **72**, 55–72.

Fehler, M. and Pearson, C. F., 1981, Acoustic radiation patterns for borehole sources: 22nd Ann. Symp., Soc. Prof. Well Log Anal.

Hayashi, K., Abé, H., 1989, Evaluation of hydraulic properties of the artificial subsurface system in Higashi-Hachimantai geothermal model field: J. Geother. Res. Soc. Japan, **11**, 203–215.

Hayashi, K., Shoji, T., Niitsuma, H., Ito, T., and Abé, H., 1985, A new in-situ tectonic stress measurements and its application to a geothermal model field: Trans., Geother. Res. Counc., **9**, 99–104.

Niitsuma, H., 1989a, Fracture mechanics design and development of HDR reservoir—Concept and results of "Γ-Project": Internat. J. Rock Mech. and Min. Sci., Abstr. **26**, 169–175.

———, 1989b, Downhole AE measurement technique and its application to geothermal fields: J. Acous. Emis., **7**, 201–209.

Sato, M., Nakatsuka, K., Niitsuma, H., and Yokoyama, H., 1986, Calibration of downhole AE measuring system by detonation test: Proc. 8th Internat. AE Symp. NDI, 389–395.

APPENDIX

PRINCIPAL COMPONENT ANALYSIS TO DETERMINE THE NORMAL UNIT VECTOR

We define the $m \times n$ vector $q\mathbf{SH}_{kp} = (qx_p, qy_p, qz_p)$ $(q = 1, 2, \ldots, m)$, in terms of the observed n SH_k vectors $\mathbf{SH}_{kp} = (x_p, y_p, z_p)$ $(p = 1, 2, \ldots, n)$. The covariance matrix for the $q\mathbf{SH}_{kp}$ is represented as follows;

$$V = \begin{bmatrix} V_{xx} & V_{xy} & V_{xz} \\ V_{yx} & V_{yy} & V_{yz} \\ V_{zx} & V_{zy} & V_{zz} \end{bmatrix}, \qquad \text{(A-1)}$$

where

$$V_{xx} = \frac{1}{nm-1}\sum_{p,q}(qx_p - \bar{x})^2,$$

$$V_{yy} = \frac{1}{nm-1}\sum_{p,q}(qy_p - \bar{y})^2,$$

$$V_{zz} = \frac{1}{nm-1}\sum_{p,q}(qz_p - \bar{z})^2,$$

$$V_{xy} = V_{yx} = \frac{1}{nm-1}\sum_{p,q}(qx_p - \bar{x})(qy_p - \bar{y}),$$

$$V_{yz} = V_{zy} = \frac{1}{nm-1}\sum_{p,q}(qy_p - \bar{y})(qz_p - \bar{z}),$$

$$V_{zx} = V_{xz} = \frac{1}{nm-1}\sum_{p,q}(qz_p - \bar{z})(qx_p - \bar{x}),$$

$$\bar{x} = \frac{1}{nm}\sum_{p,q} qx_p,$$

$$\bar{y} = \frac{1}{nm}\sum_{p,q} qy_p,$$

$$\bar{z} = \frac{1}{nm}\sum_{p,q} qz_p.$$

The normal unit vector $\mathbf{n}$ of the most probable plane, which contains the observed SH_k vectors, is obtained as the eigen vector $\mathbf{u}_3$ corresponding to the minimum eigen value λ_3 of the covariance matrix.